Waning of immunity by pathogen evolution

Abstract of Ph.D. Thesis

Golsa Sayyar

Supervisor: Gergely Röst, Ábel Garab

Doctoral School of Mathematics
University of Szeged, Bolyai Institute

Szeged
2025

1. Forewords

The aim of this research is, first, to develop deterministic and stochastic models to simulate the spread of infectious diseases. Second, inspired by COVID-19, we aim to explore how immunity, shaped by pathogen evolution, influences the dynamics of outbreaks.

The motivation behind this research comes from the limitations of classical epidemiological models in capturing the complexities observed during real-world outbreaks. The COVID-19 pandemic, in particular, highlighted the dynamic nature of disease transmission, influenced by emerging variants, evolving contact patterns across time and space, and changing immunity within the population.

We begin with an overview of the fundamental SIR epidemiological model, followed by a discussion of its key features, such as equilibrium points which are essential for analyzing the model's behavior.

Then, we propose two epidemiological models of disease transmission dynamics that accounts for the emergence of new strains through virus mutations, inspired by the COVID-19 pandemic. We analyze how time varying social distancing measures and differing assumptions about cross-immunity affect disease prevalence and strain dynamics. Our findings highlight that while a sequential pattern of strain replacement occurs when immunity is only against earlier strains, more complex dynamics, such as the co-circulation of multiple strains, emerge when immunity is strain-specific. These results are compared with genomic patterns observed during the COVID-19 pandemic.

Next, we explore the application of the SIR model within network structures. We emphasize the need for stochastic modeling to capture the complexities of disease transmission, particularly in the context of COVID-19. By analyzing the dynamics of virus spread across different networks, we investigate how network features influence disease propagation. We also examine the effects of viral mutations and immunity on transmission patterns, and evaluate the effectiveness of social distancing strategies in controlling outbreaks.

Finally, we address the challenge of predicting viral evolution by developing a novel model by considering a trade-off between immunity evasion and transmissibility. The model identifies that highly transmissible strains tend to evolve toward immune evasion, while less contagious strains shift toward increased transmissibility. By assuming a linear trade-off, we derive a non-linear difference equation to describe long-term evolutionary patterns. Our analysis provides criteria for evolutionary convergence, identifies cycli-

cal patterns in strain evolution, and reveals conditions under which viral evolution becomes chaotic.

2. Introduction

A simple SIR model with demography is obtained by the following system, where each equation describes the rate of change of the compartments over time [1]:

$$\begin{aligned} \dot{S}(t) &= -\beta S(t)I(t) + \mu - \mu S(t), \\ \dot{I}(t) &= \beta S(t)I(t) - \gamma I(t) - \mu I(t), \\ \dot{R}(t) &= \gamma I(t) - \mu R(t). \end{aligned} \tag{1}$$

The generation of susceptible individuals in this model is given by recruitment rate $\mu > 0$, which also equals the per capita death rate. They become infected at rate $\beta S(t)I(t)$, and infected individuals recover at rate $\gamma I(t)$.

The basic reproduction number is defined as $\mathcal{R}_0 = \frac{\beta}{\gamma+\mu}$. The disease-free equilibrium is given by $(S^*, I^*, R^*) = (1, 0, 0)$. If $\mathcal{R}_0 > 1$, the model admits a biologically meaningful endemic steady state that is asymptotically stable:

$$(S^*, I^*, R^*) = \left(\frac{1}{\mathcal{R}_0}, \frac{\mu}{\beta}(\mathcal{R}_0 - 1), \frac{\gamma}{\beta}(\mathcal{R}_0 - 1) \right). \tag{2}$$

3. Epidemic patterns of emerging variants with dynamical social distancing

Motivated by the emergence of new variants during the COVID-19 pandemic, we propose two scenarios that arise under different assumptions regarding cross-immunity.

3.1. ***First Scenario: One-Way Cross-Immunity Towards Earlier Variants***

In this scenario, individuals who have recovered from strain j ($j = 1, 2, \ldots, n$) are fully immune to any strain i where $i \leq j$, but they have no immunity to subsequent strains.

In the early stage of the epidemic, no social distancing measures are in place ($\sigma = 1$). Subsequently, when the infected population reaches a threshold of L/γ (corresponding to a daily incidence of L), we implement social distancing measures to stabilize the infected population at this fixed

level, $\sum_{j=1}^{n} I_j = L/\gamma$. As the number of infections from the initial strain diminishes due to recoveries, the newly emerged strains will sequentially replace the previous ones in dominance (left hand side of Fig. 3.1).

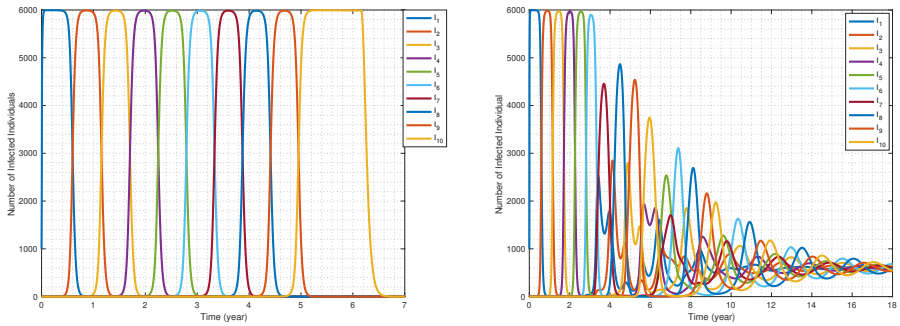

Figure 3.1: Infected population of each strain of Scenario 1 (left) and Scenario 2 (right). $N = 10^6$, $L = 1500$, $\gamma = 0.25$, $\beta = 7.5 \times 10^{-7}$.

We also highlight the impact of the daily number of allowable new infections on the implementation of social distancing measures over time: a higher number of newly infected individuals per day corresponds to a higher $\sigma(t)$, indicating milder interventions for social distancing. As a dominant strain wanes, we can relax the measures to some extent. However, as new strains emerge and gain prominence, stricter measures become necessary once again, leading to an oscillatory pattern in the intensity of interventions (Fig. 3.2, left).

A natural question arises: do newer strains exhibit the same dominance period as earlier ones? We illustrate that allowing more new individuals to be infected by a strain results in a shorter duration of dominance and quicker fade-out of that strain. Under this scenario, each subsequent strain exhibits a shorter period of dominance compared to the previous ones. Conversely, a higher allowed incidence corresponds to shorter dominance periods and a faster emergence of novel strains (Fig. 3.2, right).

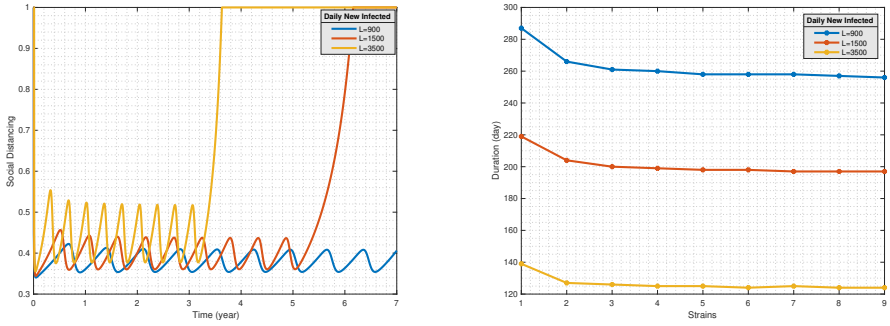

Figure 3.2: Left: Relation between social distancing parameter, σ(t), and L for ten strains of the first scenario. Right: Relation between new infections per day ($L(t)$) and duration of persistence in the population.

3.2. ***Second Scenario: Absence of Cross-Immunity***

Now, we consider a scenario where protection upon recovery from one strain provides immunity only against that particular strain. In this scenario, individuals who have recovered from a specific strain remain susceptible to both old and new strains.

In this case, unlike in Scenario 1, recovered individuals are not immune to old variants. Consequently, the behavior of the infected populations is not as regular as those under the first scenario (right hand side of Fig. 3.1).

For each strain, the infections settle around the value $L/\gamma n$ over time. In other words, for large t, we have: $I_i(t) \approx \frac{L}{\gamma n}$ for $i = 1, 2, \ldots, n$.

This phenomenon can be intuitively explained as follows: In the first scenario, susceptibility is limited to the new strains only, meaning recovered individuals cannot be infected with old strains, and there is no mutation from new strains to previous ones. Consequently, the earlier strains cannot compete with newer ones and converge to zero, while the new ones rise to L/γ.

However, in Scenario 2, each strain infects all recovered individuals, who have recovered from both new and old strains (except from the very same strain), equalizing their potential pools. Moreover, the total number of infected individuals is constrained to L/γ, which is now distributed among n equally competitive strains.

We also compare our model results with reported data on SARS-CoV-2 variants in the Netherlands during 2021–2022. The emergence and dominance of first few variants such as Alpha and Delta, closely mirrors the patterns under the Scenario 1 of our model. Notably, the durations of dominance for these variants exhibit striking similarities between the model and

the empirical data. However, starting from June 2022, a significant shift occurs, with the Omicron lineage accounting for the majority of SARS-CoV-2 variants. Within the Omicron lineage, sub-variants such as BA.5 remain prevalent, while newer sub-variants like BQ.1 are on the rise.

4. Modeling Disease Transmission in Networked Structures

Although traditional well-mixed models offer a foundational understanding of disease spread dynamics, they overlook the detailed progression of an epidemic through the diverse social and geographical settings of actual populations. Such a shortfall may result in inaccurate predictions regarding the initial outbreak and subsequent spread phases of an epidemic.

To comprehend the spread of infectious diseases within different populations, it is pivotal to explore the structure of networks that represent these populations. Two fundamental types of random networks, Scale-Free networks (SF) and Random Spatial Geometric networks (RSG), offer contrasting perspectives on network topology and its impact on disease dynamics.

4.1. ***Case Study: Tracking Infectious Diseases Across Networks***

We investigate the spread of infectious diseases by comparing the two described scenarios in Sec. 3, involving the mutation and immunity of viral strains, and analyze the transmission dynamics across two different network structures. The primary aim is to understand how these scenarios and network topologies collectively influence the patterns of disease spread and the effectiveness of interventions such as social distancing.

In both scenarios, a population of N individuals is represented as nodes in a randomly connected graph. Viral strains are organized in a circular network, where each strain can mutate to adjacent ones, with the last strain looping back to the first. This structure shapes mutation dynamics.

In the first scenario (similar to the earlier second case), mutations occur bidirectionally, i.e. strain i can mutate to $i+1$ or $i-1$, allowing continuous strain circulation. With no cross-immunity, reinfections persist, and infections from adjacent strains converge over time (Fig. 4.1 (a)).

In the second scenario (similar to the earlier first case), mutations proceed unidirectionally, it means each strain mutates only to the next, with the last strain k mutating to 1. This leads to a sequential immune buildup and eventual strain extinction due to a shrinking susceptible pool (Fig. 4.1 (b)).

Due to the RSG network's spatial structure, where nearby nodes are more likely to be connected, it exhibits a more uniform degree distribution and lacks highly connected hubs. In contrast, the SF network, formed through

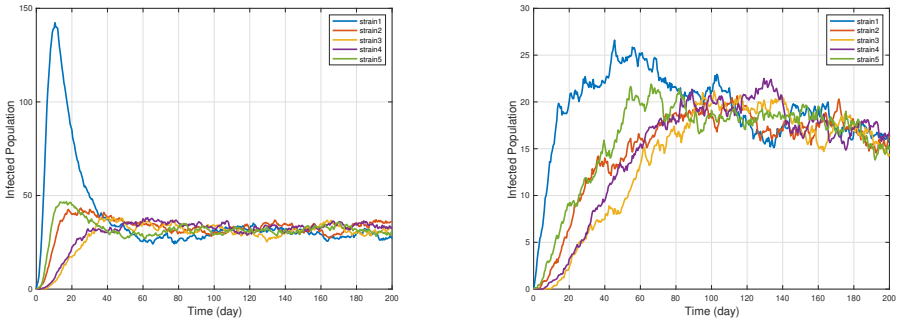

(a) Scenario 1

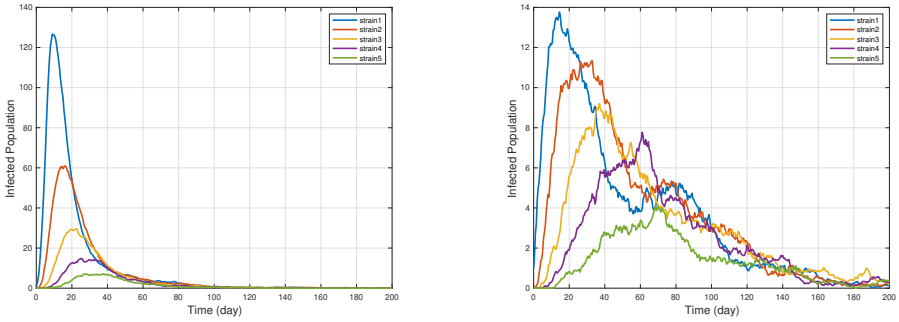

(b) Scenario 2

Figure 4.1: Comparison of epidemic spread dynamics across SF and RSG networks (left and right panels, respectively) for two scenarios. Simulations were conducted using the Gillespie algorithm with $N = 400$ nodes and 100 iterations. Both networks have the same number of edges, but the absence of hubs in the RSG network constrains transmission to local neighborhoods, slowing the spread. (a) Scenario 1: Strains can mutate to adjacent variants, and recovery does not grant immunity to other strains. SF networks show rapid transmission due to hubs, while the RSG network exhibits slower, more localized spread. (b) Scenario 2: Strains mutate sequentially, and recovery confers immunity only to previous strains. Despite equal connectivity, the RSG network again slows the epidemic due to spatial structure, while SF networks facilitate broader spread through hubs.

preferential attachment, creates hubs that accelerate disease spread. Despite having the same number of edges, transmission in the RSG network is slower, as the absence of hubs limits rapid propagation. Instead, infections spread gradually, constrained by local connectivity and spatial proximity.

4.2. ***Control Strategy for Disease Spread: Global Social Distancing***

We aim to control the spread of disease using a global social distancing strategy. This strategy is activated when the virus prevalence exceeds a predetermined threshold. At this point, all individuals reduce their contacts, regardless of infection status. In the network model, this is implemented by randomly removing a fraction σ_G of all connections.

Social distancing allows us to explore varying intervention intensities. We examine three levels: no distancing ($\sigma_G = 0$), moderate distancing ($\sigma_G = 0.4$), and high distancing ($\sigma_G = 0.7$).

In the second scenario (sequential mutation with one-way cross-immunity), global social distancing moderately reduces infection levels. However, the effectiveness is constrained by the declining pool of susceptible individuals, limiting the virus's spread. In contrast, the first scenario (dynamic mutation without cross-immunity) shows a more pronounced response, with social distancing nearly halving the infected population. The lack of cross-immunity increases the effectiveness of social distancing by limiting opportunities for reinfection with new strains.

We also observe a clear gradient in infection levels with increasing social distancing intensity. Higher levels of social distancing lead to progressively lower infected populations. This result underscores the importance of intervention measures in controlling disease spread.

The effectiveness of social distancing varies depending on the network structure. In scale-free networks, where transmission hubs are more prominent, high-intensity social distancing is especially effective. In random spatial graphs, moderate distancing suffices to achieve significant reductions in infection levels.

Finally, the timing of intervention is crucial. Implementing social distancing when only 2.5% of the population is infected, rather than waiting until 5% or 10%, accelerates outbreak control and significantly reduces infection rates.

5. Evolution into chaos – implications of the trade-off between transmissibility and immune evasion

A major concern with emerging COVID-19 variants has been their ability to evade immunity and the implications for future waves. While previous biological studies have suggested a potential trade-off between immune evasion and transmissibility, our work presents the first mathematical analysis supporting this idea.

5.1. Direction of the viral evolution: higher transmissibility or immune evasion?

We consider the SIR Model (1) and introduce invader strains, denoted by the index v, while the system attains its endemic steady state. We aim to discern whether the emergence of this invader strain is attributable to its capacity to evade immunity or its enhanced transmissibility.

These newly emerging strains differ from the resident strain in two distinct ways:

- Immune Evasion: Invader strains have the capability to evade immunity and infect individuals who have recovered from the resident strain (R). To quantify this, we introduce the parameter $p \in [0, 1]$ which represents the fraction of recovered individuals from the resident strain that can be infected by the new strain.
- Transmissibility: Invader strains may exhibit either heightened or diminished contagiousness relative to the resident strain. This is delineated by the parameter $\beta_v = \beta + f(p)$, where $f(p)$ represents the trade-off function between transmissibility and immune evasion. This trade-off function operates under the following assumptions:

(H1) f is continuously differentiable on $[0, 1]$;

(H2) $f'(p) < 0$, for $p \in [0, 1]$;

(H3) $f(0) > 0$ and $f(1) < 0$.

The early dynamics associated with the invader strain, represented by linearization at the endemic equilibrium, and characterized by the transmission rate β_v, can be expressed as follows:

$$\dot{I}_v(t) = \beta_v S^* I_v(t) + \beta_v p R^* I_v(t) - \gamma I_v(t) - \mu I_v(t). \tag{3}$$

Therefore, the invasion reproduction number for the invader strains when the resident strain is in its endemic steady state, is

$$\mathcal{R} = \frac{(\beta + f(p))(S^* + pR^*)}{\gamma + \mu} = \frac{\beta + f(p)}{\gamma + \mu}\left[\frac{(\mu + \gamma)}{\beta} + \frac{p\gamma(\beta - (\mu + \gamma))}{\beta(\mu + \gamma)}\right], \quad (4)$$

which denotes the number of secondary infections produced by an individual infected with the invasive variant over the course of their infectious period, within a population where resident strains have achieved equilibrium [3].

The subsequent theorem states that when β is small, the invasion reproduction number is a monotone decreasing function of p, indicating the emergence of a new strain with a higher transmission rate. Conversely, in case of high transmission rate β, circumventing the immune system is the most advantageous evolutionary strategy for the invader strain.

Theorem 1. *Let f satisfy (H1)–(H3). We assume the resident strain of model (1) is in its endemic steady state, as given by (2). Then, there exists sufficiently small $\delta > 0$ such that if $\beta \in (\mu + \gamma, \mu + \gamma + \delta)$, then the invasion reproduction number $\mathcal{R}(p)$ decreases on $[0, 1]$, and it attains its maximum at $p = 0$ and $\beta_v = \beta + f(0)$. For large values of β, $\mathcal{R}$ is an increasing function of p on $[0, 1]$, hence the maximum of $\mathcal{R}(p)$ occurs at $p = 1$ and $\beta_v = \beta + f(1)$.*

Now, we direct our attention towards identifying and closely examining the most invasive strain, i.e. the strain with the maximal invasion fitness. Therefore, we focus on answering the question of how this strain can maximize its reproduction number in presence of the resident strain.

To facilitate the mathematical analysis throughout the remainder of this research, we employ a linear trade-off f with transmission advantage parameter a, and cost parameter b representing the expense of immunity evasion: $f(p) = a - bp$, where $0 < a < b$.

The maximum point of $\mathcal{R}(p)$ is given by

$$p^{\max}(\beta) = \begin{cases} 0, & \beta < \tilde{\beta}_1 \\ \frac{\beta + a}{2b} - \frac{(\mu+\gamma)^2}{2\gamma(\beta-(\mu+\gamma))}, & \tilde{\beta}_1 \leq \beta \leq \tilde{\beta}_2 \\ 1, & \beta > \tilde{\beta}_2, \end{cases} \quad (5)$$

where

$$\tilde{\beta}_1 = \frac{\mu + \gamma - a}{2} + \frac{\sqrt{\gamma^2(\mu + \gamma + a)^2 + 4b\gamma(\mu + \gamma)^2}}{2\gamma}$$

and

$$\tilde{\beta}_2 = \frac{\mu+\gamma-a+2b}{2} + \frac{\sqrt{\gamma^2(\mu+\gamma+a-2b)^2+4b\gamma(\mu+\gamma)^2}}{2\gamma}.$$

This new fittest strain is characterized by a novel transmission rate denoted as $\beta_v = \beta + a - bp^{\max}$, and from this point on, it takes the place of the resident strain in the system.

By iterating this procedure, we obtain a sequence of transmission rates driven by the difference equation

$$\beta_{n+1} = g(\beta_n), \quad \beta_0 > \gamma + \mu, \tag{6}$$

where $g : (\gamma+\mu, \infty) \to (\gamma+\mu, \infty)$,

$$g(\beta) = \begin{cases} \beta + a, & \text{if } \beta < \tilde{\beta}_1; \\ \frac{\beta+a}{2} + \frac{b(\mu+\gamma)^2}{2\gamma(\beta-(\mu+\gamma))}, & \text{if } \tilde{\beta}_1 \le \beta \le \tilde{\beta}_2; \\ \beta + a - b, & \text{if } \beta > \tilde{\beta}_2. \end{cases} \tag{7}$$

We, then, demonstrate a variety of behaviors, from stability, through periodicity, to chaos.

5.2. ***Global Convergence***

Through the mathematical framework presented below, Theorem 2, we investigate the conditions under which transmissibility is stabilized, implying that over the long term, emerging variants will have approximately the same transmission rate. We illustrate this by providing explicit conditions under which the emergence of forthcoming strains, characterized by the sequence of transmission rates $\{\beta_n\}$, converges to the fixed point.

Theorem 2. *The unique fixed point β^* of the difference equation (6) is*

(i) locally asymptotically stable (LAS) if

$$b > a > \gamma + \mu \quad \text{or} \quad b > \max\left\{a, \frac{3\gamma(\gamma+\mu-a)^2}{4(\gamma+\mu)^2}\right\};$$

(ii) locally unstable if $a < b < \frac{3\gamma(\gamma+\mu-a)^2}{4(\gamma+\mu)^2}$ and $a \le \gamma + \mu$;

(iii) globally asymptotically stable (GAS) (i.e. LAS and globally attractive) if

$$b > a > \gamma+\mu \;\; or \;\; b > \max\left\{a, \frac{3\gamma(\gamma+\mu-a)^2}{4(\gamma+\mu)^2}, \frac{3\gamma(-a^2+4(\gamma+\mu)^2)}{16(\gamma+\mu)^2}\right\}.$$

Fig. 5.1 illustrates the bifurcation diagram of the function $g(\beta)$ with b serving as the bifurcation parameter. This diagram reveals how varying the parameter b leads to changes in solutions of the difference equation (6), representing the sequence of transmission rates of emerging fittest strains. The pink and orange lines mark the critical points of b for local and global stability, respectively (under the condition $a < \gamma + \mu$). Surpassing the threshold of local stability given by Theorem 2(i), solutions demonstrate convergence towards the fixed point. This means, over a sufficiently long period, all prevailing strains will practically have the same transmission rate.

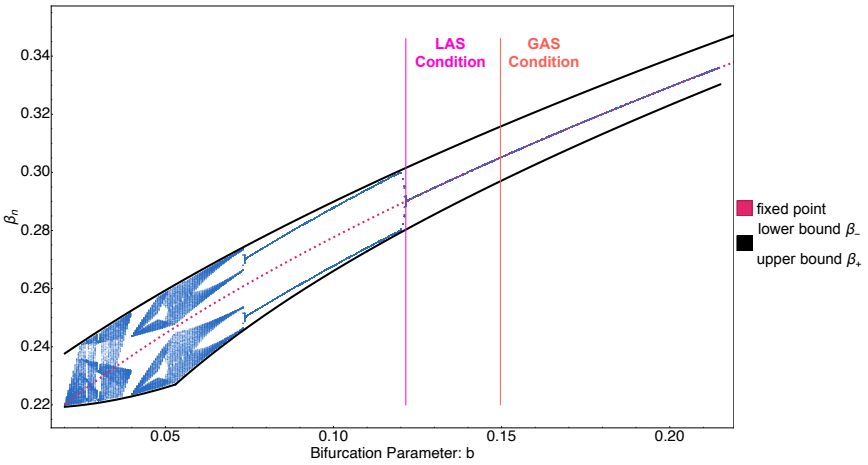

Figure 5.1: Bifurcation diagram for the difference equation (6). The diagram captures the diverse behaviors—chaotic, periodic, and convergent—across a range of values for b. On the left side of the "LAS Condition"-line, the fixed point is unstable and on the right side of the "GAS Condition"-line, the fixed point is globally asymptotically stable (Theorem 2(iii)). All trajectories are confined within the interval $[\beta_-, \beta_+]$ (Theorem 3). The system was iterated for $n = 1000$ steps from ten initial values for each b in between 0.02 and 0.21 with step-size 0.0005, and the last 50 iterations are displayed in the plot. Here, $\mu = 3.5 \cdot 10^{-5}$, $\gamma = 0.2$, and $a = 0.02$.

5.3. *Attracting Interval*

In the upcoming theorem, we identify an interval into which all solutions of the difference equation (6) enter and do not leave thereafter. This implies that, over an extended period, the transmission rates of the new strains remain within this specified interval.

Theorem 3. *Let* $\beta_+ > \sup g\big((\gamma+\mu, \beta^*]\big)$ *and* $\gamma+\mu < \beta_- < \inf g\big([\beta^*, \beta_+]\big)$. *Then* $g\big([\beta_-, \beta_+]\big) \subseteq [\beta_-, \beta_+]$, *and every solution of* (6) *enters* $[\beta_-, \beta_+]$ *without leaving it again.*

5.4. *Periodic Solutions and Complex Dynamics*

Now, we demonstrate that, in cases where the fixed point is locally unstable, there is at least one two-periodic solution. These findings indicate that, despite multiple iterations and the emergence of numerous subsequent strains, only two transmission rates are repeated alternately in the system over the long term. In addition, within Theorem 5, we demonstrate that the difference equation (6), under specific conditions, exhibits chaotic behavior. This implies that the system's dynamics is unpredictable, making it challenging to forecast whether the emergence of the next strain will be attributed to a heightened transmission rate or its capability to evade the immune system.

Theorem 4. *If* $a < b < \frac{3\gamma(\gamma+\mu-a)^2}{4(\gamma+\mu)^2}$ *and* $a \leq \gamma+\mu$, *then, there exists at least one two-periodic solution of the difference equation* (6) *different from* β^*.

Theorem 5. *Let* $0 < a < b$. *If* $g(\tilde{\beta}_1+a) \leq \tilde{\beta}_1 - a$ *or* $\tilde{\beta}_2+b-a \leq g(\tilde{\beta}_2+a-b)$ *holds, then the difference equation* (6) *is chaotic in the sense of Li and Yorke [2], i.e.*

1. *for every positive integer* k *there is a periodic point in* $(\gamma+\mu, \infty)$ *having period* k;

2. *there is an uncountable set* $S \subseteq (\gamma+\mu, \infty)$ *with no periodic points which satisfies the following conditions:*

   (i) for every $p, q \in S$ *with* $p \neq q$,

   $$\limsup_{n\to\infty} |g^n(p) - g^n(q)| > 0 \quad \textit{and} \quad \liminf_{n\to\infty} |g^n(p) - g^n(q)| = 0;$$

   (ii) for every $p \in S$ *and periodic point* $q \in (\gamma+\mu, \infty)$,

   $$\limsup_{n\to\infty} |g^n(p) - g^n(q)| > 0.$$

Corollary 6. *If either* $\tilde{\beta}_2 - \tilde{\beta}_1 \leq a \leq \frac{b}{3}$ *or* $a + \tilde{\beta}_2 - \tilde{\beta}_1 \leq b \leq \frac{3a}{2}$ *is satisfied, then the difference equation* (6) *is chaotic in the sense of Li and Yorke.*

Fig. 5.2 illustrates four distinct regions, each representing a different dynamical behavior of the equation (6). The blue and yellow regions denote the domains where the fixed point is globally and locally asymptotically stable, respectively, whereas the green region highlights areas of instability where 2-periodic orbits emerge, as delineated in Theorems 2 and 4. The gray region (obtained in Theorem 5 (gray) and Corollary 6 (light gray region)) reflects the chaotic aspects of the difference equation (6), within which predicting the behavior of subsequent strains becomes challenging.

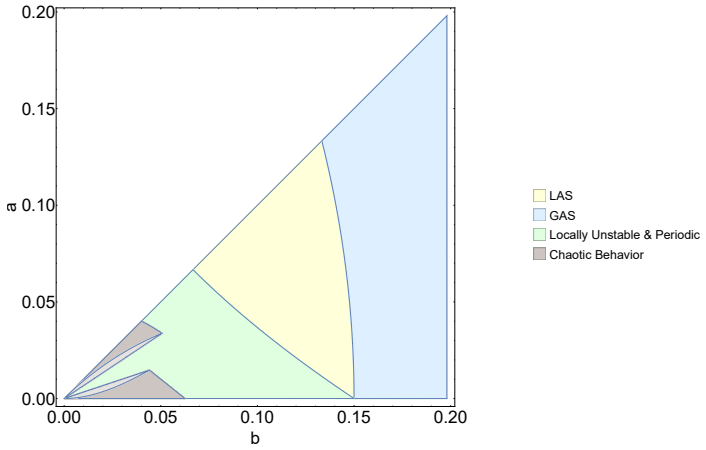

Figure 5.2: The figure delineates four distinct regions, each corresponding to a unique dynamical behavior of the system as defined by the difference equation (6). The regions colored in blue and yellow represent domains where the fixed point exhibits global and local asymptotic stability, respectively. The green regions are zones of instability, as given in Theorem 2. The area depicted in gray encapsulates chaotic dynamics of (6). Here $\gamma = 0.2$ and $\mu = 3.5 \cdot 10^{-5}$.

This dissertation is based on two articles of the author. These publications are the following:

1. Sayyar, G., and Röst, G. (2023) Epidemic Patterns of Emerging Variants with Dynamical Social Distancing. *In: Mondaini, R.P. (eds) Trends in Biomathematics: Modeling Epidemiological, Neuronal, and Social Dynamics. BIOMAT 2022. Springer, Cham, 215–232.* https://doi.org/10.1007/978-3-031-33050-6_13

2. Sayyar, G., Garab, Á., Röst, G. (2025) Evolution into chaos – implications of the trade-off between transmissibility and immune evasion. *Infectious Disease Modelling 10(3), 909–923.* https://doi.org/10.1016/j.idm.2025.04.003.

References

[1] Bauch, C. T. (2008). The Role of Mathematical Models in Explaining Recurrent Outbreaks of Infectious Childhood Diseases. *In: Brauer, F., van den Driessche, P., Wu, J. (eds) Mathematical Epidemiology. Lecture Notes in Mathematics, Springer, Berlin, Heidelberg 1945, 297–319.* https://doi.org/10.1007/978-3-540-78911-6_11

[2] Li, T. Y. and Yorke, J. A. (1975) Period three implies chaos. *The American Mathematical Monthly, 82(10), 985–992.* https://doi.org/10.2307/2318254

[3] Mitchell, C., and Kribs, C. (2019) Invasion reproductive numbers for periodic epidemic models. *Infectious Disease Modelling 4, 124-141.* https://doi.org/10.1016/J.IDM.2019.04.002